Journal of Alzheimer's Disease 31 (2012) 285–300
DOI 10.3233/JAD-2012-112198
IOS Press

Cerebellar Amyloid-β Plaques: Disturbed Cortical Circuitry in AβPP/PS1 Transgenic Mice as a Model of Familial Alzheimer's Disease

Selene Lomoio[a,b], Irene López-González[b], Ester Aso[b], Margarita Carmona[b], Benjamín Torrejón-Escribano[c], Elda Scherini[a] and Isidro Ferrer[b,*]
[a]*Dipartimento di Biologia e Biotecnologie "Lazzaro Spallanzani", Laboratorio di Biologia Cellulare e Neurobiologia, Università di Pavia, Pavia, Italy*
[b]*Institut de Neuropatologia, IDIBELL-Hospital Universitari de Bellvitge, Universitat de Barcelona, Hospitalet de Llobregat; CIBERNED (Centro de Investigación Biomédica en Red de Enfermedades Neurodegenerativas), Catalunya, Spain*
[c]*Serveis Científico-Tecnics, Unitat de Biología de Bellvitge, Universitat de Barcelona, Hospitalet de Llobregat, Catalunya, Spain*

Handling Associate Editor: Irina Alafuzoff

Accepted 9 April 2012

Abstract. Cerebellar amyloid-β (Aβ) deposition in the form of neuritic plaques and Purkinje cell loss are common in certain pedigrees of familial Alzheimer's disease (FAD) mainly linked to *PS1* mutations. *AβPP/PS1* transgenic mice, here used as a model of FAD, show a few Aβ plaques in the molecular layer of the cerebellum at 6 months, and which increase in number with age. Motor impairment is apparent in transgenic mice aged 12 months. Combined methods have shown degenerated parallel fibers as the main component of dystrophic neurites of Aβ plaques, loss of synaptic contacts between parallel fibers and dendritic spines of Purkinje cells, and degeneration of granule cells starting at 12 months and increasing in mice 18/20 months old. In addition, abnormal mitochondria and focal loss of Purkinje and basket cells, together with occasional axonal torpedoes and increased collaterals of Purkinje cells in mice aged 18/20 months, is suggested to be a concomitant defect presumably related to soluble extracellular or intracellular Aβ. These observations demonstrate serious deterioration of the neuronal circuitry in the cerebellum of *AβPP/PS1* transgenic mice, and they provide support for the interpretation of similar alterations occurring in certain pedigrees with FAD.

Keywords: *AβPP/PS1* transgenic mice, cerebellum, familiar Alzheimer disease, parallel fibers, Purkinje cell

INTRODUCTION

Alzheimer's disease (AD) is the most common cause of cognitive impairment and dementia in old age. The neuropathological features of AD comprise neuronal loss mainly in the cerebral cortex and hippocampus accompanied by the presence of amyloid-β (Aβ) plaques and neurofibrillary tangles, the two main

*Correspondence to: Isidro Ferrer, Institut de Neuropatologia, Servei d'Anatomia Patològica, Hospital Universitari de Bellvitge, carrer Feixa Llarga s/n, 08907 Hospitalet de Llobregat, Spain. Tel.: +34 93 260 7452; Fax: +34 93 260 7503; E-mail: 8082ifa@gmail.com.

histopathological hallmarks of the disease [1, 2]. The majority of cases are sporadic (sAD), but a percentage of AD is triggered by dominant genetic factors as in Down syndrome (chromosome 21 trisomy) and in familial cases with autosomal dominant inheritance (familial AD: FAD) caused by mutations in the amyloid-β protein precursor (*AβPP*) gene on chromosome 21, the presenilin-1 (*PS1*) gene on chromosome 14, and the presenilin-2 gene on chromosome 1 [3].

The cerebellar cortex may be involved at advanced stages of sAD showing diffuse Aβ deposits, but with the absence of neurofibrillary tangles and loss of Purkinje cells [4–7]. Cerebellar alterations appear earlier and are more severe in FAD, being characterized, in addition to Purkinje cell loss, by the presence of neuritic plaques [8–12]. However, little is known about the consequences on cortical cerebellar circuitry resulting from cerebellar Aβ deposition, and their possible implications in cerebellar dysfunction in AD and, particularly, in FAD.

Double-transgenic *AβPP/PS1* mice express a chimeric mouse/human AβPP (Mo/HuAβPP695swe: AβPP Swedish mutation) and a mutant human presenilin 1 (PS1-dE9), both directed to central nervous system neurons under the mouse *PRNP*, prion protein promoter [13]. The included Swedish mutation (K595N/M596L) elevates the amount of Aβ and the mutant PS1 allele accelerates the Aβ deposition rate. Transgenic mice show impaired memory and learning performance accompanied by histopathological alterations such as Aβ plaques in the neocortex and cerebellum [13–16]. For these reasons, *AβPP/PS1* double-transgenic mice are considered suitable models for FAD.

The present paper is aimed at identifying alterations in the circuitry of the cerebellar cortex that would permit better understanding of the alterations resulting from cerebellar extracellular Aβ deposition in the impaired cerebellar function in *AβPP/PS1* transgenic mice, with implications in FAD.

MATERIALS AND METHODS

Animals

The experiments were carried out on *AβPP/PS1* mice and wild-type (WT) littermates. The generation of mice expressing the human mutated forms AβPPswe and PS1dE9 has already been described [17]. Identification of transgenic mice was carried out by PCR of genomic DNA isolated from 1 cm tail clips as proposed by the Jackson Laboratories. Animals were maintained under standard animal housing conditions in a 12 h dark-light cycle with free access to food and water. Experiments were carried out according to ethical guidelines (European Communities Council Directive 86/609/EEC) and approved by the local ethics committee (UB-IDIBELL).

Human cases

The cerebellum of three cases bearing mutations in *PS1* with neuritic plaques [17] and four advanced sAD cases with diffuse cerebellar plaques were examined for immunohistochemistry in paraffin sections.

Motor function

Motor function was evaluated in mice aged 6 and 12 months (11 *AβPP/PS1* mice from different litters and 8 WT littermates per age) with two different behavioral paradigms: the wire hanging test and the rotarod. For the wire-hanging test, the apparatus consisted of a coat hanger (50 cm long; 2 mm in diameter) suspended 32 cm above a sawdust-covered surface. Latency-to-fall was measured from the time animals were placed hanging by their forepaws on the wire until they fell, with a maximum time of 1 min. Three days after the exposure to the wire hanging test, animals were placed in the rotarod (Rotamex 4/8; Columbus Instruments, OH, US). The apparatus consisted of a plastic roller (3 cm in diameter) with small grooves running along its turning axis. Mice received four trials per day for two consecutive days. During each test session, animals were placed on the rod rotating at a constant speed (4 rpm), and then the rod started to accelerate continuously from 4 to 40 rpm over 600 s. The latency-to-fall off the rotarod was recorded. The improvement in the motor coordination throughout the different trials was calculated as the difference between the latency-to-fall in each trial with respect to the first one. A criterion of a minimum latency-to-fall of 10 s during the last trial was established in order to classify animals depending on their ability to exhibit motor function in the rotarod.

Data were analyzed with Student's *t*-test. χ^2 analysis was performed to compare the percentage of mice that acquired motor coordination criteria in the rotarod between the different experimental groups. In all the experiments, the significance level was set at $p < 0.05$.

Histological procedures

Animals aged 6, 12, and 18/20 months were examined for the chronological appearance of cerebellar Aβ

plaques (3 *AβPP/PS1* mice and 3 WT per time-point). With this aim the number of plaques per section was counted in 5 sections per animal.

However, further histological studies were centered in animals aged 12 months ($n = 4$) and 18/20 months ($n = 3$), and corresponding age-matched control littermates ($n = 3$ per time-point). *AβPP/PS1* mice and control animals were deeply anesthetized by intraperitoneal injection (0.2 mL/10 g body weight) with a mixture of ketamine (100 mg/kg) and xylazine (20 mg/kg) prior to intra-cardiac perfusion with 4% paraformaldehyde in PBS delivered at a pressure of 19 mL/min. Brains were removed and post-fixed in the same fixative for 4 h. The cerebella were dissected and embedded in paraffin. Ten-μm-thick mid-sagittal sections were collected on slides and used for the morphometric and morphological analyses.

Morphometric analysis

The morphometric analysis was performed on digital images of sections of cerebellar vermis immunostained for calbindin (3 *AβPP/PS1* mice and 3 WT littermates and 5 sections per animal), captured using an Olympus camera mounted on an Olympus BX51 microscope at 4X magnification. All images were analyzed using the NIH ImageJ software.

The average area of cerebellar cortex in mm^2 was obtained by outlining the contour of sections. The data were analyzed with Student's *t*-test. The significance level was set at $p < 0.05$.

For Purkinje cell counts, the total number of Purkinje cells per section was counted and the depth of the Purkinje cell layer measured. The Purkinje cell linear density was obtained by dividing the number of Purkinje cells by the depth of the layer. Statistical evaluation of differences was performed by means of the two-level nested ANOVA on ranks test.

Morphological analysis

Light microscopy immunohistochemistry: For immunohistochemistry the following antibodies were used: mouse anti-Aβ IgG (1 : 50, Dako, DK), rabbit anti-GFAP serum (1 : 500, Dako, DK), voltage dependent anion channel (VDAC) (1 : 100, Calbiochem, Spain), Iba1 rabbit polyclonal antibody for microglia (1 : 250, Wako, Richmond, VA, US), rabbit anti-calbindin serum (1 : 5,000; CB38, Swant, CH), rabbit anti-calretinin serum (1 : 800, Chemicon, MA, US), mouse anti-parvalbumin IgG (1 : 1,000, Sigma, MO, US), mouse anti-neuronal pentraxin 1 IgG (1 : 100, a generous gift of Dr. R. Trullas, Barcelona, Spain), rabbit anti-phospho-SAPK/JNK serum (Thr183/Tyr185; 1 : 25, Cell Signaling, MA, US), rabbit anti-phospho-tau serum (Ser 199, and Thr 231; 1 : 100, Chemicon, DE), rabbit anti-α-synuclein serum (1 : 500, Chemicon, DE), mouse anti-synaptophysin IgG (1 : 500, Dako, DK), rabbit anti-ubiquitin serum (1 : 500, Dako, DK), and rabbit anti-active-caspase-3 serum (1 : 25, Cell Signaling, Beverly, MA, US).

Two slides per animal were used for each immunoreaction. After de-waxing, sections were boiled with citrate buffer for 20 min to enhance antigenicity. Sections for Aβ immunocytochemistry were pre-treated with 98% formic acid for 3 min. The endogenous peroxidases were blocked by incubation in 10% methanol-1% H_2O_2 solution for 5 min. To block unspecific sites, sections were incubated with 3% normal horse serum for 1 h. Incubation with the primary antibodies was carried out at 4°C overnight. The immunoreaction was revealed with biotinylated secondary antibodies (Dako, DK), followed by EnVision+ system peroxidase (Dako, DK) and 3′,5′-diaminobenzidine tetrahydrochloride. Some sections were incubated only in buffer instead of primary antibodies; no immunostaining was detected in these sections.

In situ end-labeling of nuclear DNA fragmentation (TUNEL) was carried out as previously reported [18] using cerebellar sections of x-irradiated newborn rats (2 Gy) killed 6 h after irradiation as positive controls. The same controls were used for immunocytochemistry to active caspase 3.

Human cases were processed in the same way excepting double-labeling immunohistochemistry to Aβ and VDAC, in which the peroxidase reaction of Aβ was visualized with diaminobenzidine, NH_4NiSO_4 and H_2O_2. The immunoreaction results in a blue-grey precipitate.

Immunofluorescence and confocal microscopy: The following antibodies were used for immunofluorescence: mouse anti-Aβ IgG (1 : 50, Dako, DK), rabbit anti-GFAP serum (1 : 500, Dako, DK), rabbit anti-calbindin serum (1 : 5,000; CB38, Swant, Switzerland), rabbit anti-calretinin serum (1 : 800, Chemicon, Billerica, MA, US), guinea-pig anti-vesicular glutamate transporter 1 (VGluT1) serum (1 : 50, Frontier Science, JP), and mouse anti-neurofilament 200 kDa IgG (RT97; 1 : 50, Novocastra, UK).

To block lipofuscin fluorescence, de-waxed sections were stained with a saturated solution of Sudan black B (Merck, DE) for 30 min. After treatment with citrate buffer to enhance antigenicity, the sections were incubated at 4°C overnight with combinations of primary antibodies. Sections for Aβ immunocytochemistry

were pre-treated with 98% formic acid for 3 min. After washing, the sections were incubated with the appropriate secondary antibodies conjugated with Alexa488, Alexa546, or Alexa633 (1 : 400, Molecular Probes, CA, US). After counterstaining of nuclei with DRAQ5™ (1 : 2,000, Biostatus, UK), the sections were mounted in Immuno-Fluore mounting medium (ICN Biomedicals, CA, US), sealed, and dried overnight. Sections were examined with a Leica TCS-SL confocal microscope.

The quantitative estimation of co-localized antigens was performed calculating the 'co-localization coefficients' on plotted cytofluorograms [19]. The data were analyzed with Student's *t*-test. The significance level was set at $p < 0.05$.

Transmission electron microscopy

AβPP/PS1 and WT mice aged 12 and 18/20 months ($n = 3$ per age and group) were deeply anaesthetized and perfused with 4% paraformaldehyde and 0.1% glutaraldehyde in PBS. Sagittal sections of cerebellar vermis (1 mm thick) were post-fixed in 1% OsO_4 for 2 h and embedded in Epon 812. Semithin sections were stained with toluidine blue and ultrathin sections with uranyl acetate and lead with citrate. Samples were examined with a Jeol Jem 1011 electron microscope.

RESULTS

Motor function

AβPP/PS1 mice exhibited preserved motor function at the age of 6 months but decreased motor function in both the wire hanging and the rotarod tests at the age of 12 months. For this reason, no further tests were carried out on animals older than one year. In the wire-hanging test, the fall latency of *AβPP/PS1* mice was significantly lower (−55%) than in WT mice ($p < 0.05$) (Fig. 1a). In addition, *AβPP/PS1* mice exhibited less improvement in the rotarod test throughout the consecutive trials. However, differences between *AβPP/PS1* and WT mice were not statistically significant in any test trial (Fig. 1b). The percentage of animals that reached the motor coordination criterion in the rotarod after 8 trials was 75% for WT mice and 27% in the *AβPP/PS1* group, revealing a significant ability reduction in transgenic animals ($p < 0.05$) (Fig. 1c).

Gross changes in the cerebellum

Measurement of the mid-sagittal section area revealed that the cerebellar vermis of *AβPP/PS1* mice

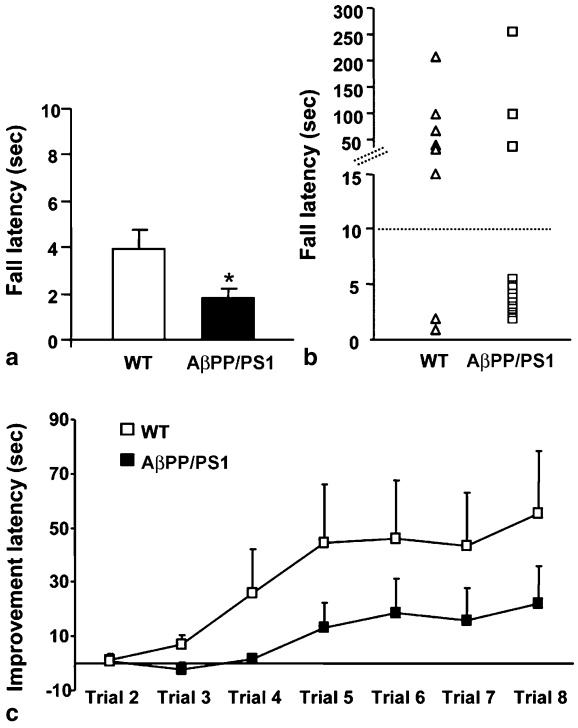

Fig. 1. Behavioral testing of the motor function of *AβPP/PS1* mice in comparison with age-matched WT at 12 months. a) In the wire hanging test, transgenic mice exhibit a significant decrease in the latency-to-fall with respect to WT animals. b) Deterioration of motor function in transgenic animals is manifested by reduced skills in rotarod performance throughout eight consecutive trials. c) Latency-to-fall of each experimental animal during the last test trial in the rotarod. Only three of the eleven *AβPP/PS1* mice reached the motor function criterion in the rotarod (minimum latency-to-fall of 10 s, dotted line), revealing impairment in the motor function of transgenic mice compared to WT littermates ($p < 0.05$). Data are expressed as mean ± SD. *$p < 0.05$, compared to WT mice (Student's *t*-test).

was smaller than the cerebellum of their WT littermates. A 20% reduction was found in transgenic mice when compared with age-matched controls at the age of 18/20 months (WT versus *AβPP/PS1*: $9.96 \pm 0.16\,mm^2$ versus $8.35 \pm 0.33\,mm^2$, $p < 0.01$).

General microscopical findings

In the cerebellum of 6-month-old *AβPP/PS1* mice, very few Aβ deposits were observed, and these were exclusively found in the molecular layer (ML). Aβ deposits were frequent in the ML in 12-month-old mice (Fig. 2). A few Aβ deposits were also present in the internal granular layer immediately beneath the Purkinje cell layer. The number of deposits increased with disease progression in mice aged 18/20 months, the last time-point examined (Fig. 3A–C). Aβ deposits

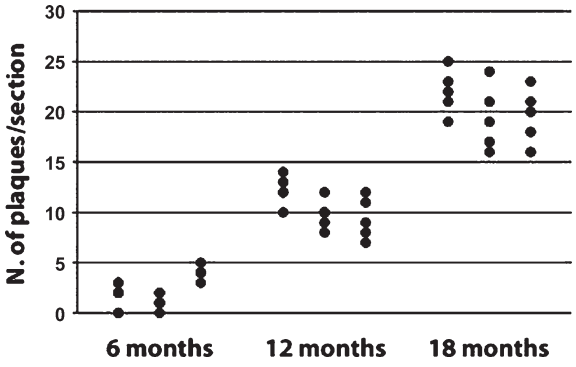

Fig. 2. Graphic representation of single counting of Aβ plaques (number of plaques/section, ordinate) obtained in 5 sections per animal, immunostained for Aβ. The maximum value obtained for each age-point does not overlap with the minimum value for the subsequent age-point.

were not observed in WT mice. At early stages, Aβ extracellular deposits were mainly diffuse; a few neuritic plaques were observed at 12 months, whereas such neuritic plaques were predominant at the age of 18/20 months. Neuritic plaques were characterized by a central core of Aβ surrounded by microglia (Fig. 3D) and astrocytes, and by dystrophic neurites clearly visualized with antibodies to mitochondrial porin VDAC (Fig. 3E), synaptophysin (Fig. 3F), among other proteins.

Cotton-wool plaques as seen in FAD cases due to PS1 mutations were not seen in *AβPP/PS1* mice. Yet Aβ angiopathy was common, involving the meningeal and cerebellar blood vessels (data not shown).

Extracellular Aβ deposits and glial cells

Extracellular Aβ deposits in the cerebellum were focal (Fig. 4a). However, astrocytes and Bergmann glial cells throughout the ML were more reactive to GFAP immunohistochemistry in *AβPP/PS1* mice aged 18/20 months when compared with age-matched WT animals (Fig. 4b, c). In addition, astrocyte processes, as identified with double-labeling immunofluorescence to Aβ and GFAP, and confocal microscopy, surrounded Aβ deposits in the ML (Fig. 4d). Furthermore, with electron microscopy, microglial cells with dense nucleus and cytoplasm filled with lysosomes and residual bodies were often encountered adjacent to dystrophic neurites surrounding Aβ plaques (Fig. 4e).

Purkinje cells

Calbindin immunohistochemistry revealed various alterations of Purkinje cells, including the presence of enlarged axons (Fig. 5a), axonal spheroids (Fig. 5b), and hypertrophic infra-ganglionic plexuses (Fig. 5c). In addition, some convolutions were devoid of Purkinje

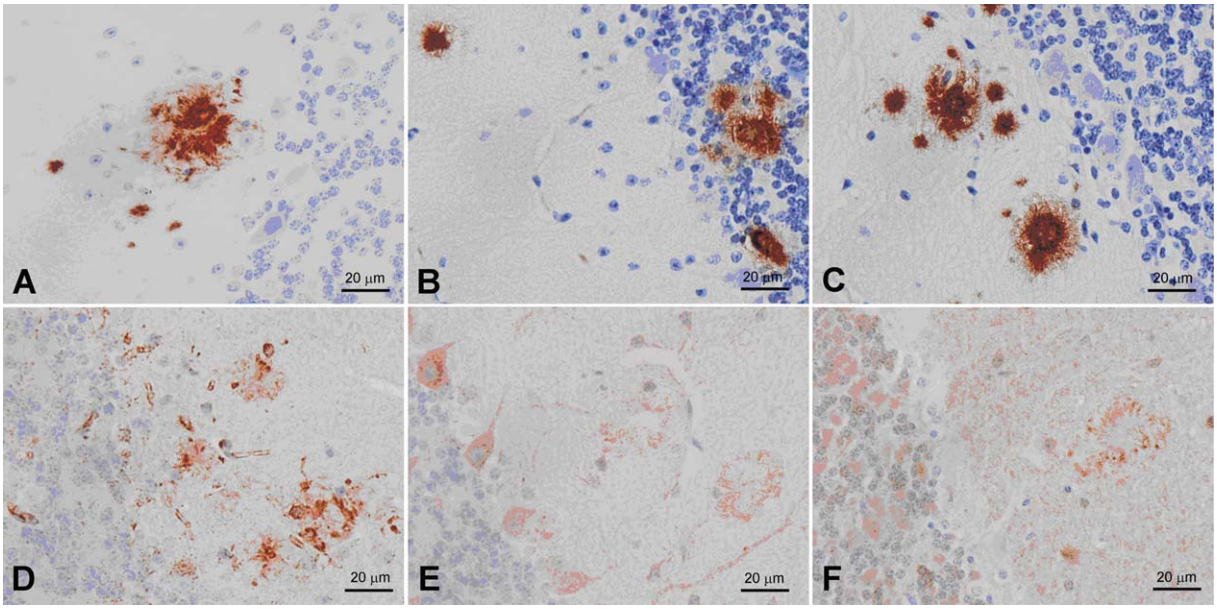

Fig. 3. Representative images of Aβ plaques in the cerebellum of *AβPP/PS1* mice aged 12 (A) and 18/20 (B, C) months, mainly located in the molecular layer but also in the granule cell layer. The majority of Aβ plaques in mice aged 18/20 months are surrounded by microglia (D) and show increased VDAC (E) and synaptophysin (F) immunoreactivity in surrounding neuronal processes characteristic of dystrophic neurites of neuritic plaques. Paraffin sections slightly counterstained with hematoxylin.

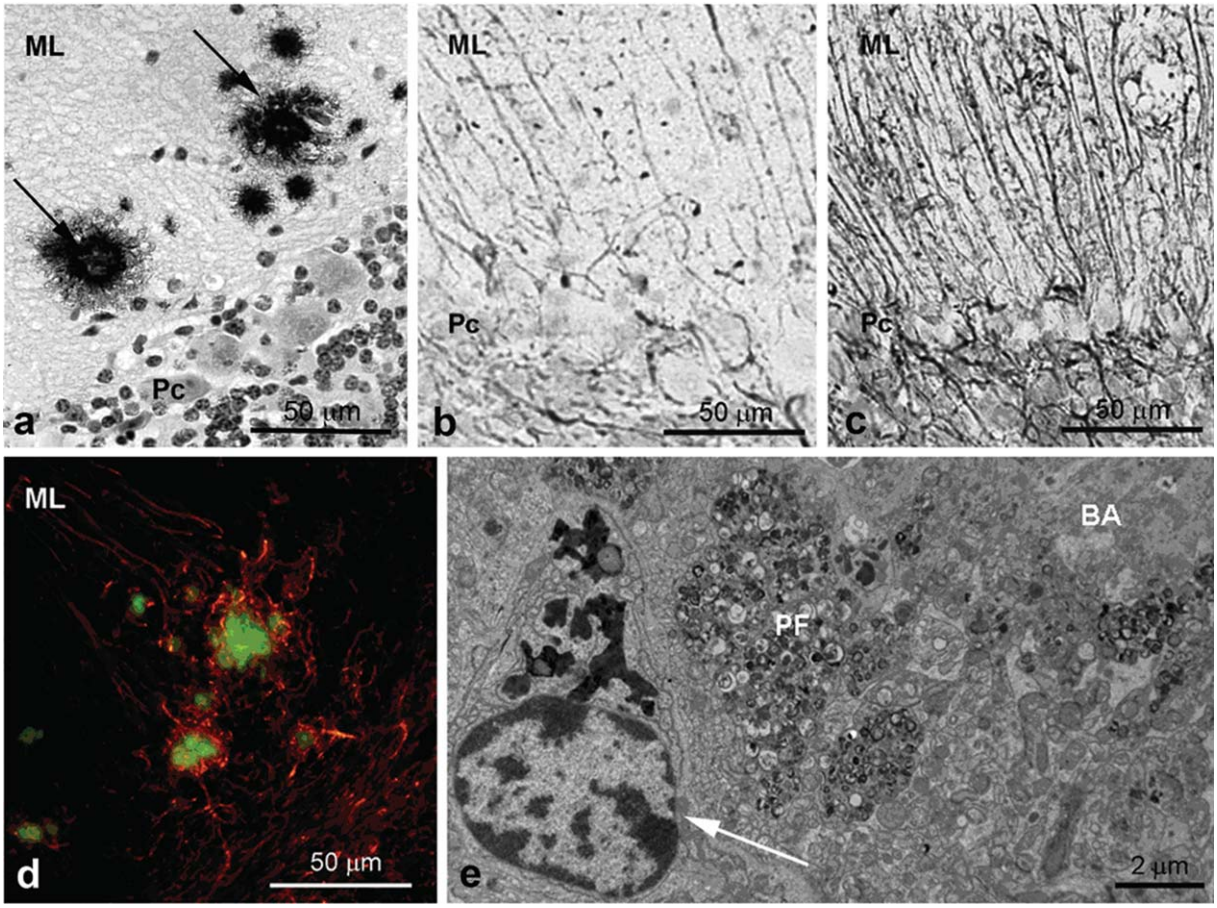

Fig. 4. Aβ plaque in the molecular layer of *AβPP/PS1* mice aged 18/20 months (a, arrows). Increased GFAP immunoreactivy is observed in the molecular layer in *AβPP/PS1* transgenic mice (c) when compared with age-matched littermates (b). Double-labeling immunofluorescence for GFAP and Aβ shows astrocytic processes (red) surrounding Aβ plaques (green) in the molecular layer (ML) (d). Electron microscopy shows a microglial cell (white arrow) adjacent to dystrophic neurites (PF) in the vicinity of an Aβ plaque. The cytoplasm of the cell is filled with lysosomes and residual bodies (d). ML = molecular layer, Pc = Purkinje cell layer, BA = Aβ.

cells (Fig. 5d). Cell counting revealed that the linear cell density of Purkinje cells was reduced by 18% and 25% in transgenic mice in comparison with WT animals at the age of 12 and 18/20 months, respectively ($p < 0.05$ and $p < 0.001$, at the ages of 12 months and 18/20 months).

Electron microscopic examination of the molecular layer revealed the presence of large mitochondria in dendrites and small branches of Purkinje cells, accompanied by occasional dark mitochondria at the ages of 12 and 18/20 months (Fig. 5e). Dendritic arbors of Purkinje cells were distorted around the amyloid deposits, as shown by double-labeling immunofluorescence to calbindin and Aβ, and confocal microscopy (Fig. 5f, g). No calbindin-immunoreactive dystrophic processes were evidenced with double-labeling immunofluorescence and confocal microscopy.

Electron microscopy of the Purkinje cell layer disclosed occasional Purkinje cells with shrunken cytoplasm and dark nuclei, and increased lipofuscin granules at the ages of 12 and 18/20 months (Fig. 5h).

Parallel fibers and granule cells

Calretinin immunohistochemistry, used as a marker of parallel fibers, revealed dystrophic terminals around Aβ deposits in the ML in mice aged 18/20 months (Fig. 6a). This was further demonstrated by double-labeling immunofluorescence to calretinin and Aβ and confocal microscopy (Fig. 6b, c). Electron microscopy revealed the dystrophic nature of these processes,

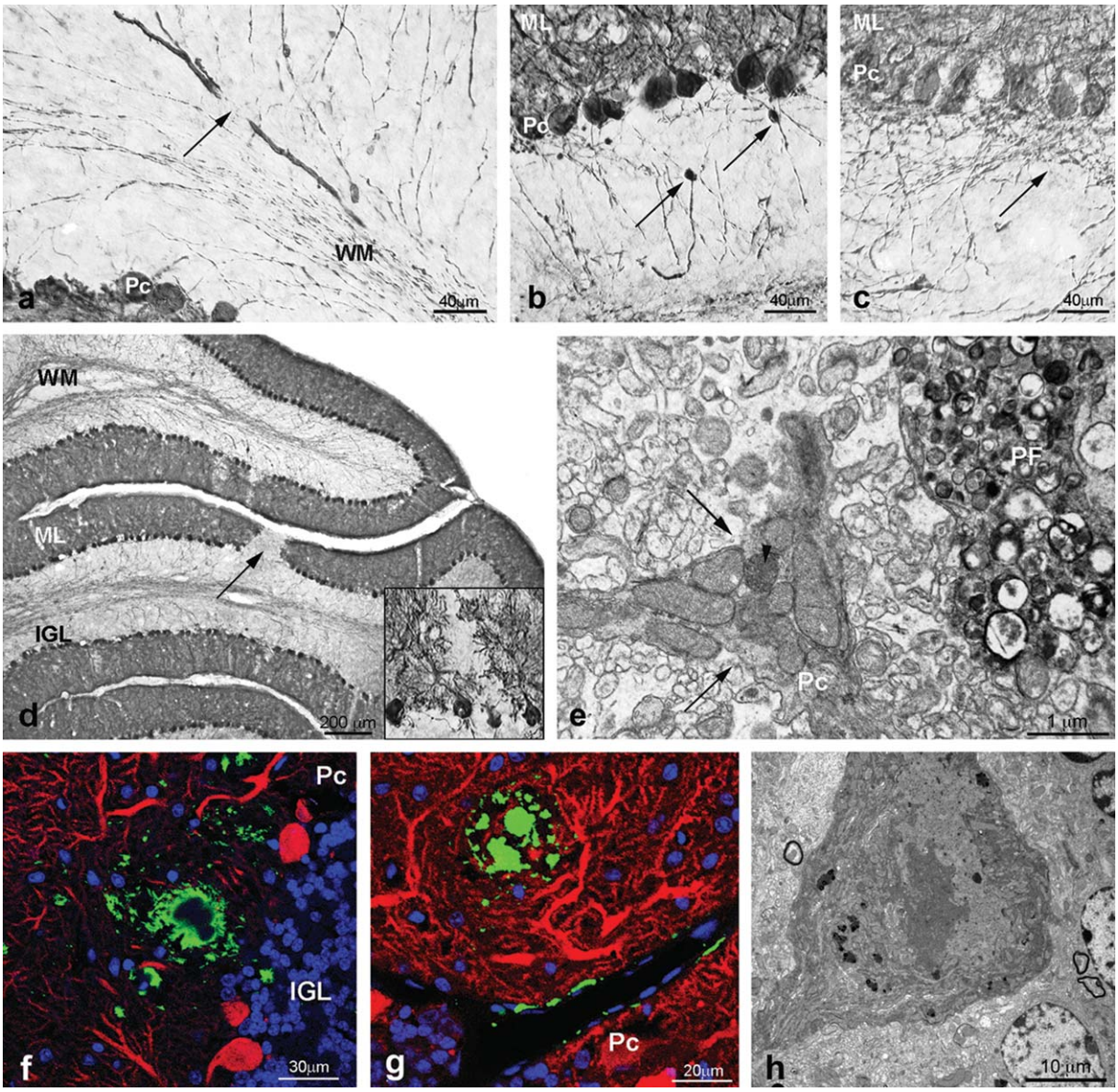

Fig. 5. Calbindin immunohistochemistry in *AβPP/PS1* mouse cerebellum aged 18/20 months shows enlarged Purkinje cell axons in the white matter (a, arrow), axonal spheroids: torpedoes (b, arrows), and hypertrophic infra-ganglionic plexuses (c, arrow). Focal loss of Purkinje cells and corresponding arbors (d and insert) is observed in *AβPP/PS1* mice. Electron microscopy shows a branch of a Purkinje cell dendrite (e, arrows) filled with large mitochondria and occasional electron-dense mitochondria (arrowhead) in the vicinity of dystrophic neurite (PF). Double-labeling immunofluorescence for calbindin (red) and Aβ (green) shows Aβ plaques in the molecular layer, some of them displacing the arbors of Purkinje cells, but apparently not producing dystrophic neurites (f, g). Nuclei are stained with Draq5 (blue). Electron microscopy shows a degenerating Purkinje cell with dark nucleus and cytoplasm, and enlarged cisternae of the endoplasmic reticulum, together with increased lipofuscin deposition (h). ML = molecular layer, Pc = Purkinje cell layer, IGL = granule cell layer, WM = white matter.

showing huge processes filled with altered mitochondria, and large numbers of membrane-bound pleomorphic bodies and other debris (Fig. 6d). Since pentraxin 1 (NP1) is part of the program of apoptotic death in cerebellar granule neurons [20], antibodies to NP1 were used to detect degeneration in cerebellar dystrophic neurites. Strong NP1 immunoreactivity was observed in dystrophic neurites of the cerebellum in *AβPP/PS1* transgenic mice (Fig. 6e).

Moreover, dystrophic cell processes surrounding Aβ deposits were also immunopositive with phospho-SAPK/JNK (Fig. 6f), a stress-activated protein kinase

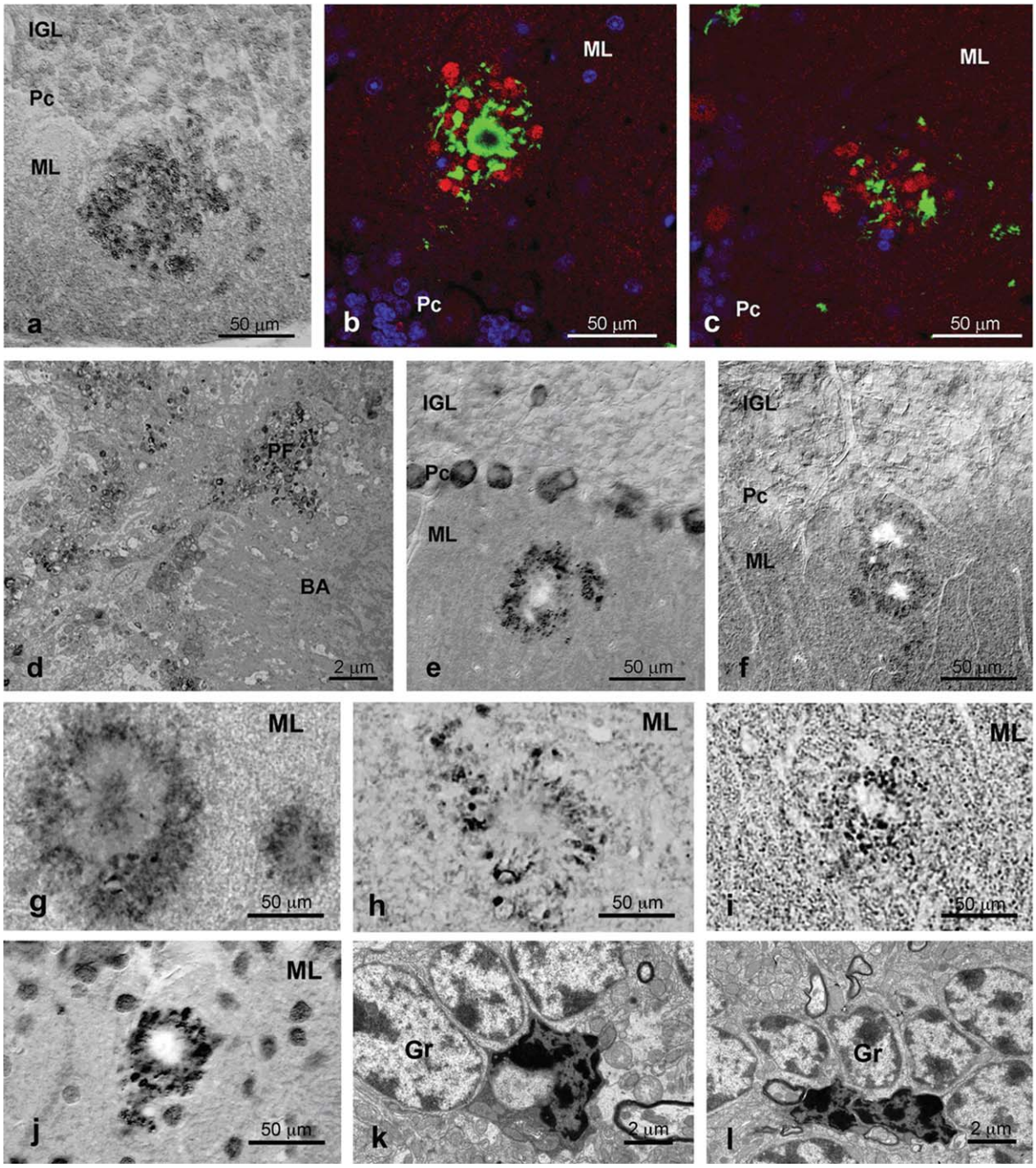

Fig. 6. Calretinin immunostaining shows positive dystrophic neurites in the molecular layer surrounding Aβ plaques in *AβPP/PS1* transgenic mice aged 18/20 months (a). Double-labeling immunofluorescence for calretinin (red) and Aβ (green), and confocal microscopy demonstrate the relationship between calretinin-immunoreactive dystrophic neurites and Aβ deposits in the molecular layer (b, c). Draq5 nuclear staining is visualized in blue. Electron microscopy shows dystrophic neurites (PF) surrounding Aβ deposits (d). Dystrophic neurites are positive for NP1 (e) and for phospho-SAPK/JNK (f), and they contain phospho-tau (g), α-synuclein (h), synaptophysin (i), and ubiquitin (j). Degenerating granule cells with condensed peripheral chromatin and dark cytoplasm contrast with the normal morphology of preserved neighboring granule cells (k, l). ML = molecular layer, Pc = Purkinje cell layer, IGL = granule cell layer, BA = Aβ, Gr = Granule cell.

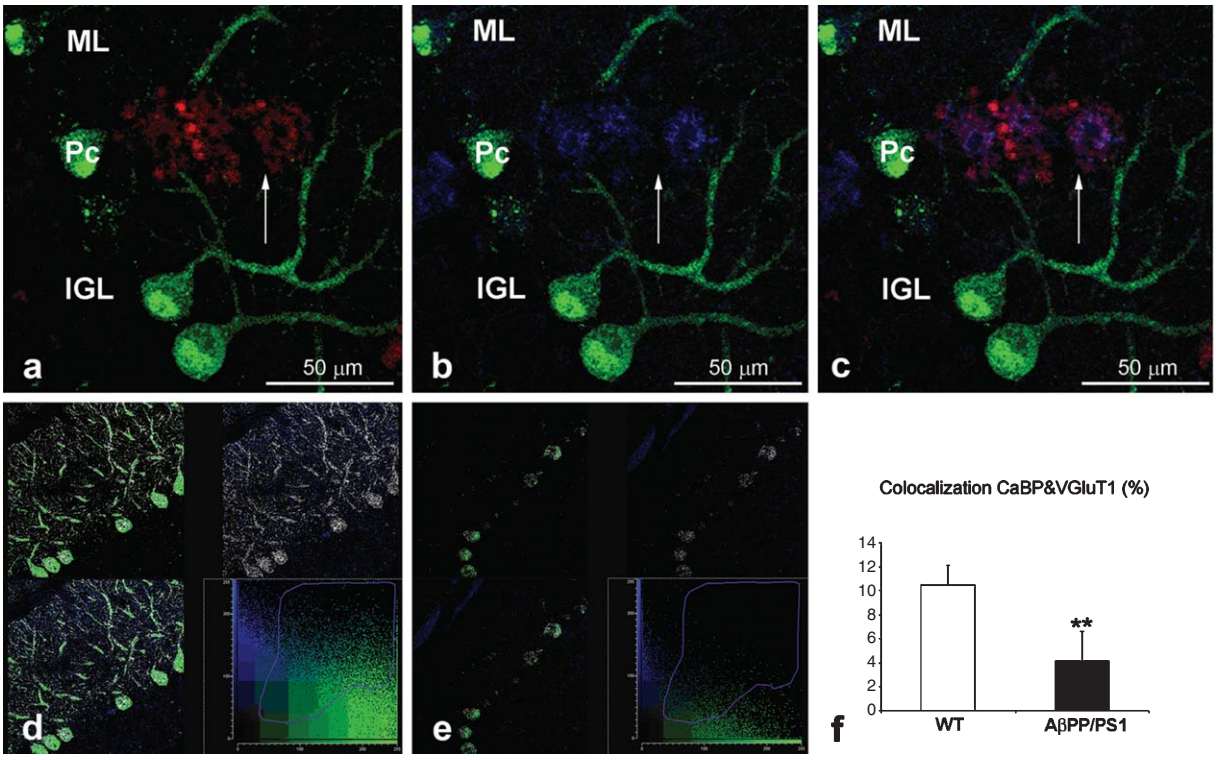

Fig. 7. Loss of synaptic contacts between parallel fibers and Purkinje cells in *AβPP/PS1* mouse cerebellum aged 18/20 months, as revealed with triple-labeling immunofluorescence and confocal microscopy to calbindin (green), calretinin (red), and the VGluT1 (blue) (a–c). Dystrophic neurites are stained with calretinin and VGluT1, demonstrating that dystrophic neurites of Aβ plaques are parallel fibers (c, merge). Cytofluorogram analysis of WT (d) and *AβPP/PS1* (e) reconstructed confocal images show a significant reduction in colocalization of calbindin with VGluT1 (−60%, f) in *AβPP/PS1* mouse cerebellum. Data are expressed as mean ± SD. $^{**}p < 0.01$, compared to WT mice (Student's *t*-test). ML = molecular layer, Pc = Purkinje cell layer, IGL = granule cell layer.

partly involved in protection against cerebellar granule cell death by regulating NP1 expression [21]. Small amounts of phospho-tau were visible around many plaques, as revealed with different phospho-specific anti-tau antibodies (Fig. 6g). In addition to phosphorylated tau, other proteins were accumulated in dystrophic neurites surrounding Aβ deposits, including α-synuclein (Fig. 6h), synaptophysin (Fig. 6i), and ubiquitin (Fig. 6j).

Electron microscopic examination of the granular layer disclosed occasional granule cells with degenerative features such as compacted peripheral chromatin and electron-dense cytoplasm (Fig. 6k, l).

Caspase 3 immunoreaction failed to show positive cells in the *AβPP/PS1* mice cerebellum. Also, after TUNEL reaction, no cells were labeled at any time-point of the study. In contrast, consistent numbers of caspase-3-immunoreactive cells and of neurons stained with TUNEL were present in the cerebella of newborn x-ray irradiated rats, killed 6 hours later, which were used as positive controls (data not shown).

Synaptic contacts between parallel fibers and Purkinje cells

By triple-labeling immunofluorescence and confocal microscopy for calbindin, calretinin, and the vesicular glutamate transporter VGluT1, a presynaptic marker of parallel fibers, calretinin-immunoreactive dystrophic neurites surrounding Aβ deposits in *AβPP/PS1* mice aged 18/20 months were stained with anti-VGluT1 antibodies, thus confirming that dystrophic neurites derived from parallel fibers (Fig. 7a–c). Moreover, the 37-plane 3 μm thick *z*-stack reconstruction of the confocal images and the cytofluorogram (Fig. 7d, e) showed a significant reduction of co-localization of calbindin with VGluT1 (calbindin versus VGluT1, −75%, $p < 0.01$; VGluT1 versus calbindin, −60%, $p < 0.05$f) in *AβPP/PS1* mice, suggesting loss of synaptic contacts between Purkinje

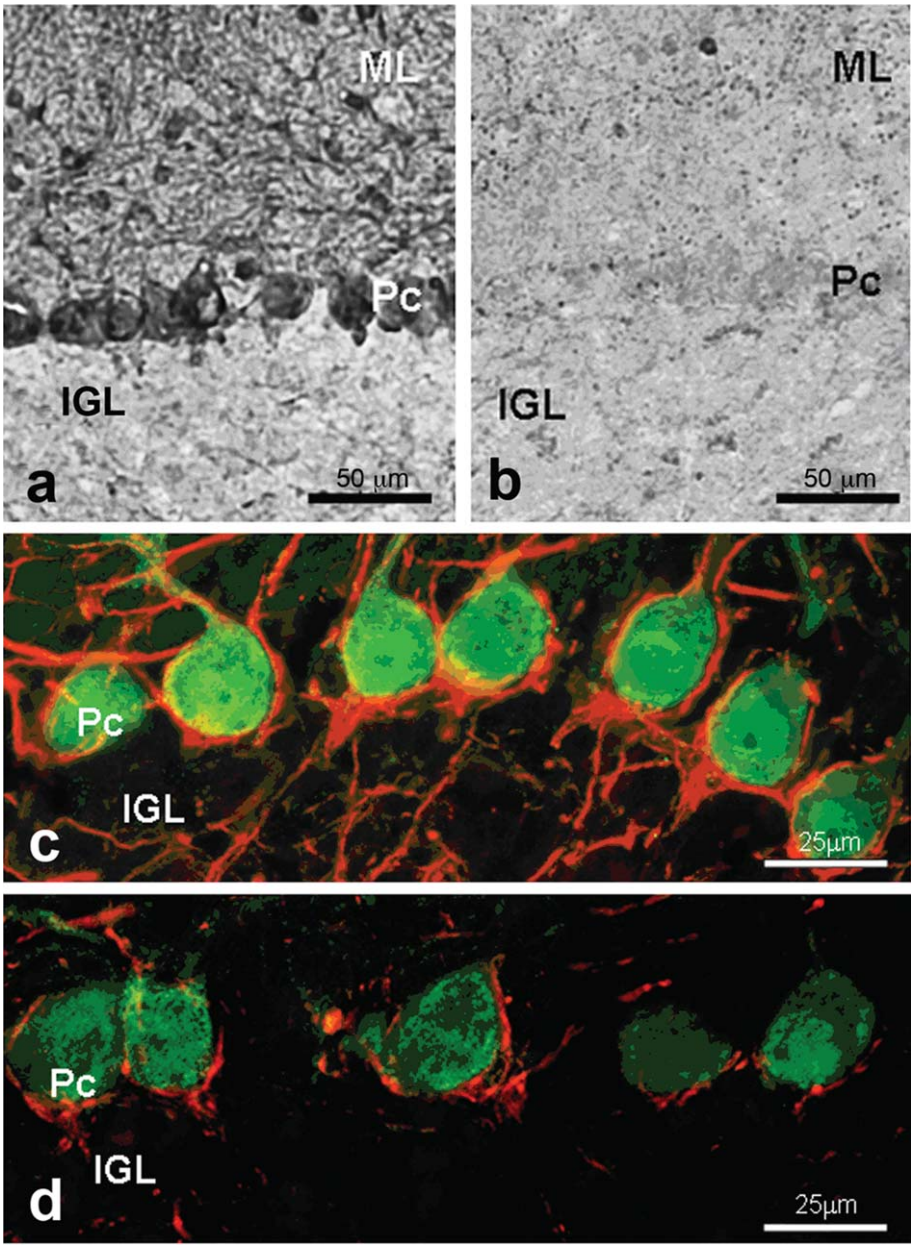

Fig. 8. Parvalbumin immunoreactivity stains Purkinje cells and local-circuit neurons of the molecular layer in normal cerebellum (a). Similar staining occurs in *AβPP/PS1* transgenic mice. However, focal loss of Purkinje cells and local-circuit neurons may occur in transgenic mice aged 18/20 months. In less affected areas, double-labeling immunofluorescence discloses focal reduction of basket plexuses, as revealed with antibody RT97 (red), surrounding Purkinje cells, as visualized with anti-calbindin antibodies (green) in transgenic mice (d) when compared with age-matched WT (c). ML = molecular layer, Pc = Purkinje cell layer, IGL = granule cell layer.

cells and parallel fibers in *AβPP/PS1* mice at the age of 18/20 months.

Basket neurons

Parvalbumin immunoreactivity was used to detect Purkinje cells and interneurons of the molecular layer. Dystrophic neurites were not stained with anti-parvalbumin antibodies. Not only Purkinje cells (as already noted) but also local-circuit neurons were lost or unstained in *AβPP/PS1* transgenic mice aged 18/20 months (Fig. 8b) when compared with WT (Fig. 8a). The consequences were best illustrated by double-labeling immunofluorescence to calbindin and RT97,

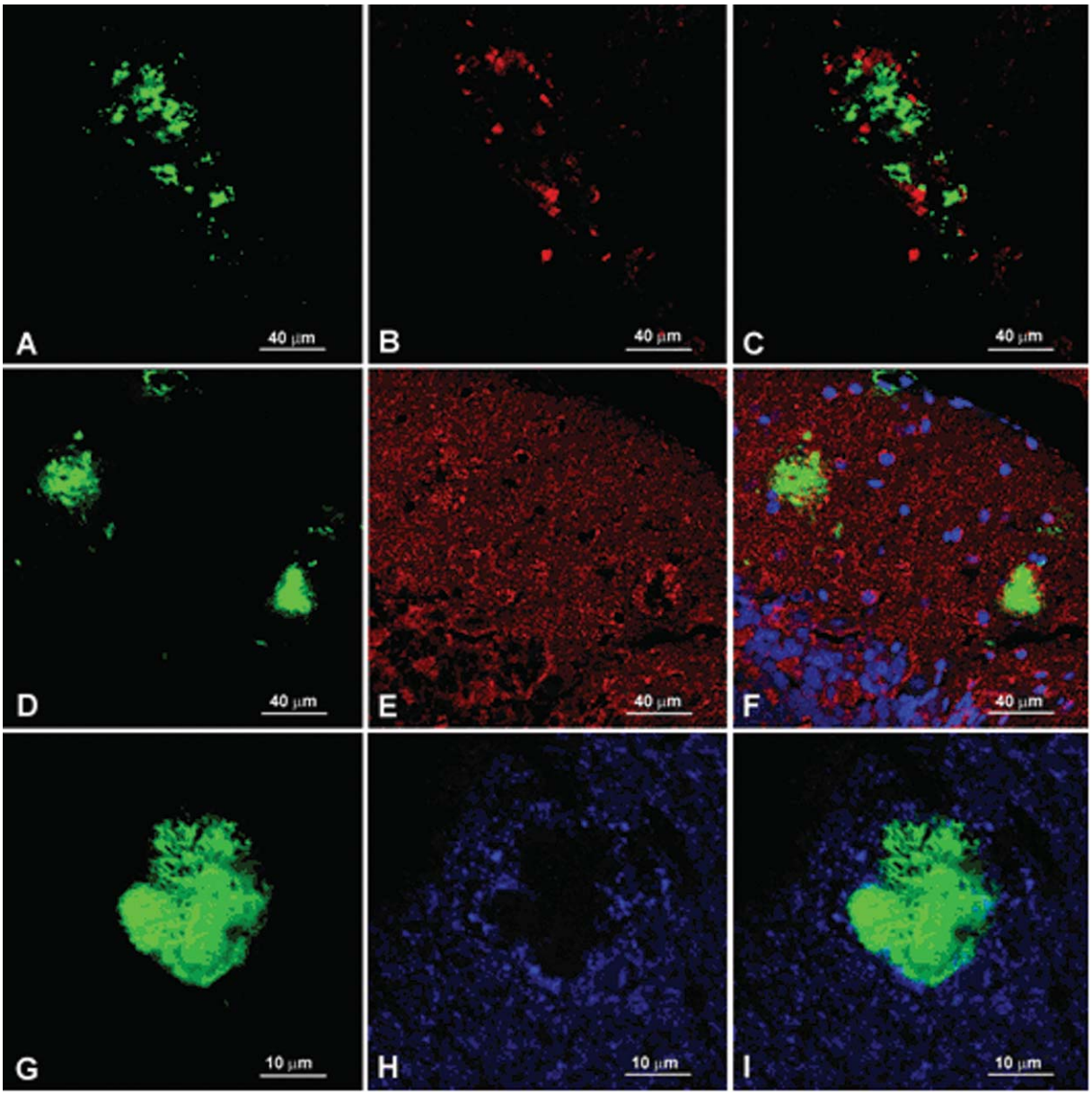

Fig. 9. Double-labeling immunofluorescence and confocal microscope to Aβ (a, d, g, green) and VDAC (b, red), calretinin (e, red) and VGluT1 (h, blue) in the molecular layer of the cerebellum of mice aged 12 months. Dystrophic neurites are seen surrounding Aβ deposits.

which decorates the axons of basket cells, showing reduced baskets around apparently preserved Purkinje cells in *AβPP/PS1* transgenic mice (Fig. 8d) when compared to controls (Fig. 8c).

Dystrophic neurites with disease progression in AβPP/PS1 mice

Similar studies were carried out in *AβPP/PS1* mice aged 12 months. Most Aβ deposits were devoid of dystrophic neurites, and, therefore, their morphology was reminiscent of diffuse plaques. However, some Aβ deposits were surrounded by dystrophic neurites. Double-labeling immunofluorescence and confocal microscopy disclosed altered neurites filled with VDAC (Fig. 9a) indicating accumulation of mitochondria, and increased expression of calretinin-immunoreactive granules (Fig. 9b) and weak enhancement in the expression of VGluT1 (Fig. 9c), thus revealing their origin in parallel fibers.

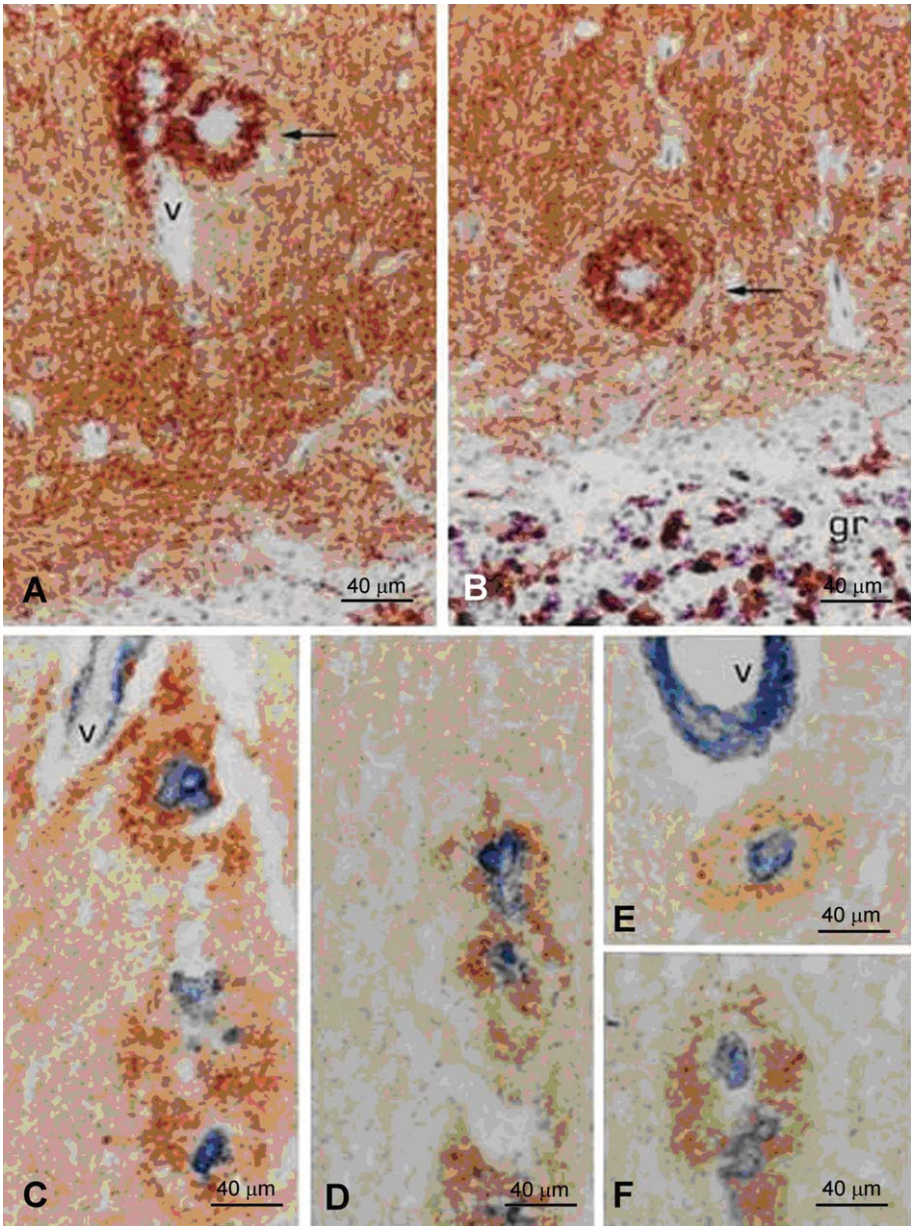

Fig. 10. FAD human cerebellum immunostained with anti-synaptophysin antibodies (A, B), and processed for double-labeling immunohistochemistry to Aβ (dark blue) and VDAC (brown) (E, F). v: blood vessel, gr: granular layer. Arrows point to the crown of dystrophic neurites. Aβ is found in the blood vessel walls and in neuritic plaques.

Neuritic plaques in the cerebellum of FAD

For comparative purposes, paraffin sections of the cerebellar vermis of sAD and FAD cases were examined for immunohistochemistry. Unfortunately, calretinin and VGluT1 antibodies did not work properly in human cases. However single- and double-labeling immunohistochemistry to synaptophysin, VDAC and Aβ disclosed enhanced synaptophysin and VDAC immunoreactivity around Aβ plaques in FAD (Fig. 10). No similar alterations were found in relation with diffuse Aβ plaques in sAD (data not shown).

DISCUSSION

Motor function was evaluated in *AβPP/PS1* and WT mice by using two common tests, the wire hanging

test and the rotarod, which demonstrate altered motor performance. It may be argued that the observations made using these methods are indicative of poor motor function that may result from causes other than cerebellar impairment, such as reduced motor strength and altered basal ganglia motor coordination. More specific methods could have been employed but morphological examination of the cerebellum promptly served to focus the study on the objective visualization of altered neurons and damaged intrinsic cerebellar pathways.

The present observations have shown increased Aβ deposition with disease progression in the cerebellar cortex of *AβPP/PS1* mice. Aβ plaques without dystrophic neurites were predominant in mice aged 12 months although a small percentage of Aβ deposits showed incipient dystrophic neurites at this age. Cerebellar Aβ deposits at advanced stages are reminiscent of Aβ neuritic plaques in the cerebral cortex and other brain regions in *AβPP/PS1* mice [14], and they are similar to those seen in the cerebellum in FAD [12]. Dystrophic neurites of Aβ plaques in the cerebellum of *AβPP/PS1* mice contain phospho-tau and several proteins including α-synuclein, synaptophysin and ubiquitin, and they are filled with abnormal mitochondria and autophagic inclusions, as are plaques of the cerebral cortex and other regions [14, 16]. This is an important point, as dystrophic neurites are a fair manifestation of altered, non-functional neuronal processes associated with Aβ deposits.

Cell composition and connectivity of the cerebellar cortex is well established [22–25]. Briefly, major afferents are the mossy fibers and climbing fibers. Mossy fibers establish excitatory synapses with dendrites of granule cells in the glomeruli; climbing fibers promote excitatory impulses in the proximal dendrites of Purkinje cells, type II Golgi cells, stellate cells, and basket neurons. Granule cells throughout the ascending axons, divided into parallel fibers in the molecular layer, form excitatory contacts with spines of dendritic arbors of Purkinje cells. The system is modulated by distinct types of local neurons covering type II Golgi cells in the granular layer which make inhibitory synapses at granule cell dendrite, and mossy fibers at the glomeruli; stellate cells in the molecular layer which are inhibitory of Purkinje cells at the dendritic arbors; and basket cells, just above the Purkinje cell layer, whose axons embrace the cell body of Purkinje cells and provide robust inhibition of these cells. Purkinje cells are inhibitory and are the only efferents of the cerebellar cortex to the deep cerebellar nuclei and vestibular nuclei.

The present observations have shown degeneration of parallel fibers associated with Aβ plaques in the molecular layer as revealed by calretinin staining and further supported by the expression of the vesicular glutamate transporter 1 (VGluT1), as a marker of parallel fibers [26]. This is associated with reduced focal synaptic contacts of parallel fibers to Purkinje cells, as shown by combined cytofluorograms. The toxic effect of Aβ on parallel fibers is further demonstrated by the observation of local over-expression of pentraxin 1 (NP1) which is associated with neuronal degeneration in AD [20], and eventual cell death under particular conditions [15]. Whether loss of parallel fibers results in the retrograde degeneration of individual granule cells, as evidenced with electron microscopy, remains to be determined, but appears likely.

In addition, other cells are altered without apparent direct contact with Aβ deposition. This was seen by using antibodies against calbindin and parvalbumin as markers of Purkinje cells and other local cortical cerebellar neurons [27, 28]. Quantitative studies have shown a 25% decrease of Purkinje cells in *AβPP/PS1* mice aged 18/20 months. In addition, abnormalities of Purkinje cells include changes of dendritic arbors in the molecular layer, axonal torpedoes, increased axon collaterals, and, importantly, the presence of large mitochondria mainly in the dendritic arbors, even at the thin terminal *branchlets.* Similar mitochondrial changes are not seen in normal Purkinje cells [24]. Focal loss of basket cells is shown by focal loss of parvalbumin-immunoreactive cells just above the Purkinje cell layer and by the reduced number of basket terminals around the soma of groups of Purkinje cells.

Since loss of Purkinje cells and axonal torpedoes, and loss of basket cells, is not physically related to Aβ plaques, it can be suggested that they are the consequence of other factors rather than of the presence of plaques. In this line, several studies have shown that soluble Aβ oligomers are causative of neurodegeneration [29–34], and that maintenance of Aβ oligomers does not impair disease progression in spite of Aβ plaque depletion [35].

Increased soluble Aβ has been demonstrated in the cerebral cortex of *AβPP/PS1* mice [14, 36], and the level of $A\beta_{42}$ is higher than the level of $A\beta_{40}$ in the frontal cortex, hippocampus, and cerebellum in these mice [36].

Furthermore, intracellular AβPP and Aβ are observed in AD under appropriate staining conditions [37]. Microdissected human neurons analyzed by a sensitive ELISA have shown increased intracellular

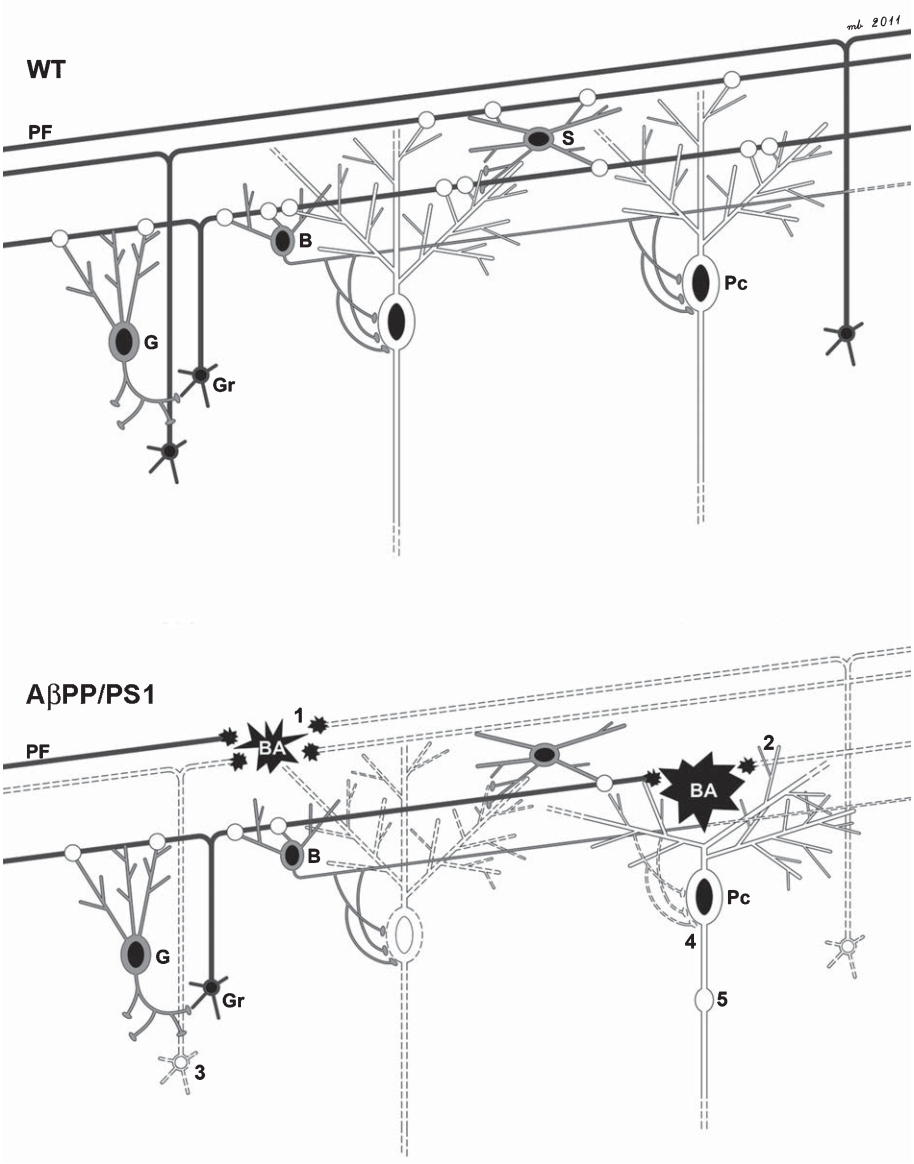

Fig. 11. Diagram showing the changes in cerebellar cortex circuitry in *AβPP/PS1* mice compared with wild type animals (WT). 1) Degeneration of parallel fibers (PF) in association with Aβ plaques (BA) in the molecular layer; 2) Focal loss of excitatory synaptic contacts following damage to parallel fibers on dendritic spines of Purkinje cells (Pc), and probably also on Golgi neurons (G), stellate (S) and basket (B); 3) Loss of granule cells presumably secondary to damage of parallel fibers; 4) Focal loss of basket cells and loss of basket terminals around Purkinje cells may account for decreased Purkinje cell inhibition; 5) Focal degeneration of Purkinje cells, altered dendritic arbors, axonal swellings (torpedoes) and increased collateral plexus, probably resulting in reduced cortical inputs to the deep cerebellar nuclei.

levels of $A\beta_{42}$ in pyramidal neurons and Purkinje cells in AD when compared with corresponding neurons in age-matched controls [38]. Therefore, although not specifically examined in the present study, it can be assumed that both extracellular soluble and intracellular Aβ are putatively harmful to cerebellar neurons in *AβPP/PS1* mice. Whether a link exists between putative intracellular Aβ and abnormal mitochondria in Purkinje cells in *AβPP/PS1* mice should be examined by using suitable experimental paradigms.

As shown in Fig. 11, morphological cerebellar abnormalities in *AβPP/PS1* transgenic mice can be enumerated as follows: i) loss of parallel fibers in association with Aβ plaques; ii) loss of synaptic contacts of granule cells to Purkinje cells as a result of focal degeneration of parallel fibers; iii) focal loss of granule

cells probably resulting from retrograde degeneration of parallel fibers; iv) focal loss of baskets probably leading to focal impairment of Purkinje cell inhibition; and v) axonal torpedoes, increased axon collaterals, and focal loss of Purkinje cells probably resulting in reduced cortical cerebellar outputs. Motor impairment is not uncommon at advanced stages of FAD due to *PS1* mutations. Spastic paraparesis and parkinsonism have been observed in several families [39–43]. Cerebellar symptoms occur in some pedigrees [43] and are marked in others [10, 12]. Although the majority of FAD cases with cerebellar involvement are associated with PS1 mutations, rare mutations in *AβPP* are manifested with generalized cerebellar Aβ deposition [9]. On the other hand, transgenic mice with *PS1* mutations alone have not shown clear AD pathology so far. Therefore, it is difficult at this moment to attribute to AβPP or to PS1 mutations their impact on the cerebellar damage in *AβPP/PS1* mice.

The present findings in *AβPP/PS1* mice, together with previous observations showing axonal degeneration in the spinal cord [44], may help to increase our understanding of motor and cerebellar impairment in certain advanced FAD cases manifested with motor and cerebellar symptoms with Purkinje cell loss and abundant Aβ neuritic plaques.

ACKNOWLEDGMENTS

This study was supported by the European Commission's 7th Framework Programme under GA No 278486, "DEVELAGE". We thank S. Juvés for care and genotyping of the animals, M. Bonato for the diagram design, and T. Yohannan for editorial help.

Authors' disclosures available online (http://www.j-alz.com/disclosures/view.php?id=1260).

REFERENCES

[1] Duyckaerts C, Dickson DW (2003) Neuropathology of Alzheimer's disease. In: *Neurodegeneration: The molecular pathology of dementia and movement disorders*. Dickson DW, ed., ISN Neuropath Press, Basel, pp. 47-65.

[2] Lowe J, Mirra SS, Hyman B, Dickson DW (2008) Ageing and dementia. In: *Greenfield's Neuropathology*, vol 1. Love S, Louis DN, Ellison DW, eds., Hodder Arnold, London, pp. 1031-1152.

[3] Bettens K, Sleegers K, Van Broeckhoven C (2010) Current status of Alzheimer disease molecular genetics: From past, to present, to future. *Hum Mol Genet* **19**(R1), R4-R11.

[4] Dickson DW, Wertkin A, Mattiace LA, Fier E, Kress Y, Davies P, Yen SH (1990) Ubiquitin immunoelectron microscopy of dystrophic neurites in cerebellar senile plaques of Alzheimer's disease. *Acta Neuropathol* **79**, 486-493.

[5] Mavroudis IA, Fotiou DF, Adipepe LF, Manani MG, Njau SD, Psaroulis D, Costa VG, Baloyannis SJ (2010) Morphological changes of the human Purkinje cells and deposition of neuritic plaques and neurofibrillary tangles on the cerebellar cortex of Alzheimer's disease. *Am J Alzheimers Dis Other Demen* **25**, 585-591.

[6] Thal DR, Rub U, Orantes M, Braak H (2002) Phases of A beta-deposition in the human brain and its relevance for the development of AD. *Neurology* **58**, 1791-1800.

[7] Wegiel J, Wisniewski HM, Dziewiatkowski J, Badmajew E, Tarnawski M, Reisberg B, Mlodzik B, De Leon MJ, Miller DC (1999) Cerebellar atrophy in Alzheimer's disease—clinicopathological correlations. *Brain Res* **818**, 41-50.

[8] Fukutani Y, Cairns NJ, Rossor MN, Lantos PL (1996) Purkinje cell loss and astrocytosis in the cerebellum in familial and sporadic Alzheimer's disease. *Neurosci Lett* **214**, 33-36.

[9] Giaccone G, Morbin M, Moda F, Botta M, Mazzoleni G, Uggetti A, Catania M, Moro ML, Redaelli V, Spagnolki A, Rossi RS, Salmona M, DiFede G, Tagliavini F (2010) Neuropathology of the recessive A673V APP mutation: Alzheimer disease with distinctive features. *Acta Neuropathol* **120**, 803-812.

[10] Lemere CA, Lopera F, Kosik KS, Lendon CL, Ossa J, Saido TC, Yamaguchi H, Ruiz A, Martinez A, Madrigal L, Hincapie L, Arango JC, Anthony DC, Koo EH, Goate AM, Selkoe DJ, Arango JC (1996) The E280A presenilin 1 Alzheimer mutation produces increased A beta 42 deposition and severe cerebellar pathology. *Nat Med* **2**, 1146-1150.

[11] Lopera F, Ardilla A, Martinez A, Madrigal L, Arango-Viana JC, Lemere CA, Arango-Lasprilla JC, Hincapie L, Arcos-Burgos M, Ossa JE, Behrens IM, Norton J, Lendon C, Goate AM, Ruiz-Linares A, Rosselli M, Kosik KS (1997) Clinical features of early-onset Alzheimer disease in a large kindred with an E280A presenilin-1 mutation. *JAMA* **277**, 793-799.

[12] Sepulveda-Falla D, Matschke J, Bernreuther C, Hagel C, Puig B, Villegas A, Garcia G, Zea J, Gomez-Mancilla B, Ferrer I, Lopera F, Glatzel M (2011) Deposition of hyperphosphorylated tau in cerebellum of PS1E280A Alzheimer's disease. *Brain Pathol* **21**, 452-463.

[13] Borchelt DR, Thinakaran G, Eckman CB, Lee MK, Davenport F, Ratovitsky T, Prada CM, Kim G, Seekins S, Yager D, Slunt HH, Wang R, Seeger M, Levey AI, Gandy SE, Copeland NG, Jenkins NA, Price DL, Younkin SG, Sisodia SS (1996) Familial Alzheimer's disease linked presenilin 1 variants elevate Abeta1-42/1-40 ratio *in vitro* and *in vivo*. *Neuron* **17**, 1005-1011.

[14] Aso E, Lomoio S, López-González I, Joda L, Carmona M, Fernández-Yagüe N, Moreno J, Juvé S, Pujol A, Pamplona R, Portero-Otin M, Martín V, Díaz M, Ferrer I (2011) Amyloid generation and dysfunctional immunoproteasome activation with disease progression in animal model of familial Alzheimer disease. *Brain Pathol*, doi: 10.1111/j.1750-3639.2011.00560.x.

[15] Blanchard V, Moussaoui S, Czech C, Touchet N, Bonici B, Planche M, Canton T, Jedidi I, Gohin M, Wirths O, Bayer TA, Langui D, Duyckaerts C, Tremp G, Pradier L (2003) Time sequence of maturation of dystrophic neurites associated with Abeta deposits in AβP/PS1 transgenic mice. *Exp Neurol* **184**, 247-263.

[16] Savonenko A, Xu GM, Melnikova T, Morton JL, Gonzales V, Wong MP, Price DL, Tang F, Markowska AL, Borchelt DR (2005) Episodic-like memory deficits in the APPswe/PS1dE9 mouse model of Alzheimer's disease: Relationships to

β-amyloid deposition and neurotransmitter abnormalities. *Neurobiol Dis* **18**, 602-617.

[17] Pera M, Alcolea D, Sánchez-Valle R, Guardia-Laguarta C, Badiola N, Suárez-Calvet M, Lladó A, Barrera-Ocampo AA, Sepulveda-Falla D, Blesa R, Molinuevo JL, Clarimón J, Ferrer I, Gelpi E, Lleó A (2012) Distinct patterns of APP processing in the CNS in autosomal-dominant and sporadic Alzheimer disease, submitted.

[18] Ferrer I, Serrano T, Rivera R, Olivé M, Zújar MJ, Graus F (1993) Radiosensitive populations and recovery in X-ray-induced apoptosis in the developing cerebellum. *Acta Neuropathol* **86**, 491-500.

[19] Manders EM, Stap J, Brakenhoff GJ, van Driel R, Aten JA (1992) Dynamics of three dimensional replication patterns during the S-phase, analyzed by double-labeling of DNA and confocal microscopy. *J Cell Sci* **103**, 857-862.

[20] Abad MA, Enguita M, DeGregorio-Rocasolano N, Ferrer I, Trullas R (2006) Neuronal pentraxin 1 contributes to the neuronal damage evoked by amyloid-beta and is overexpressed in dystrophic neurites in Alzheimer's brain. *J Neurosci* **26**, 12735-12747.

[21] Enguita M, DeGregorio-Rocasolano N, Abad A, Trullas R (2005) Glycogen synthase kinase 3 activity mediates neuronal pentraxin 1 expression and cell death induced by potassium deprivation in cerebellar granule cells. *Mol Pharmacol* **67**, 1237-1246.

[22] Carpenter MB (1991) *Core text of neuroanatomy* 4th Ed. Williams and Wilkins, Baltimore, Buenos Aires, Hong Kong, London, Munich, Philadelphia, Sydney, Tokyo.

[23] Llinás R, Hillamn DE (1969) Physiological and morphological organization of the cerebellar circuits in various vertebrates. In: *Neurobiology of cerebellar evolution and development*. Llinas R, ed., AMA-ERF Institute for Biomedical Research, Chicago, pp. 43-73.

[24] Palay SL, Chan-Palay V (1974) *Cerebellar Cortex. Cytology and Organization*. Springer-Verlag, Berlin, Heidelberg, New York.

[25] Ramón y Cajal S (1899) *Textura del Sistema Nervioso del Hombre y de los Vertebrados*. Imprenta y Librería de Nicolás Moya, Madrid. Re-edited by Instituto de Neurociencias, Universidad de Alicante, 1992.

[26] Hioki H, Fujiyama F, Taki K, Tomioka R, Furuta T, Tamamaki N, Kaneko T (2003) Differential distribution of vesicular glutamate transporters in the rat cerebellar cortex. *Neuroscience* **117**, 1-6.

[27] Bastianelli E (2003) Distribution of calcium-binding proteins in the cerebellum. *Cerebellum* **2**, 242-262.

[28] Celio MR (1990) Calbindin D-28k and parvalbumin in the rat nervous system. *Neuroscience* **35**, 375-475.

[29] Deshpande A, Mina E, Glabe C, Busciglio J (2006) Different conformation of amyloid beta induce neurotoxicity by distinct mechanisms in human cortical neurons. *J Neurosci* **26**, 6011-6018.

[30] Glabe CG, Kayed R (2006) Common structure and toxic function of amyloid oligomers implies a common mechanism of pathogenesis. *Neurology* **66**, S74-S78.

[31] McLean CA, Cherny RA, Fraser FW, Fuller SJ, Smith MJ, Beyreuther K, Bush AI, Masters CL (1999) Soluble pool of Abeta amyloid as a determinant of severity of neurodegeneration in Alzheimer's disease. *Ann Neurol* **46**, 860-466.

[32] Ono K, Yamada M (2011) Low-n oligomers as therapeutic targets of Alzheimer's disease. *J Neurochem* **117**, 19-28.

[33] Shankar GM, Li S, Metha TH, Garcia-Muñoz A, Shepardson NE, Smith I, Brett FM, Farrell MA, Rowan MJ, Lemere CA, Regan CM, Walsh DM, Sabatini BL, Selkoe DJ (2008) Amyloid-beta protein dimers isolated directly from Alzheimer's brains impair synaptic plasticity and memory. *Nat Med* **14**, 837-842.

[34] van Helmond Z, Miners JS, Kehoe PG, Love S (2010) Oligomeric Aβ in Alzheimer's disease: Relationship to plaque and tangle pathology, APOE genotype and cerebral amyloid angiopathy. *Brain Pathol* **20**, 468-480.

[35] Nicoll JA, Barton E, Boche D, Neal JW, Ferrer I, Thompson P, Vlachouli C, Wilkinson D, Bayer A, Games D, Seubert P, Schenk D, Holmes C (2006) Abeta species removal after abeta42 immunization. *J Neuropathol Exp Neurol* **65**, 1040-1048.

[36] Xiong H, Callaghan D, Wodzinska J, Xu J, Premyslova M, Liu QY, Connelly J, Zhang W (2011) Biochemical and behavioral characterization of the double transgenic mouse model (APPswe/PS1dE9) of Alzheimer's disease. *Neurosci Bull* **27**, 221-232.

[37] Aho L, Pikkarainen M, Hiltunen M, Leinonen V, Alafuzoff I (2010) Immunohistochemical visualization of amyloid-beta protein precursor and amyloid-beta in extra- and intracellular compartments in the human brain. *J Alzheimers Dis* **20**, 1015-1028.

[38] Hashimoto M, Bogdanovic N, Volkmann I, Aoki M, Winblad B, Tjernberg LO (2010) Analysis of microdissected human neurons by a sensitive ELISA reveals a correlation between elevated intracellular concentrations of Aβ42 and Alzheimer's disease neuropathology. *Acta Neuropathol* **119**, 543-554.

[39] Brooks WS, Kwok JB, Kril JJ, Broe GA, Blumbergs PC, Tannenberg AE, Lamont PJ, Hedges P, Schofiled PR (2003) Alzheimer's disease with spastic paraparesis and 'cotton wool' plaques: Two pedigrees with PS-1 exon deletions. *Brain* **126**, 783-791.

[40] Houlden H, Baker M, McGowan E, Lewis P, Hutton M, Crook R, Wood NW, Kumar-Singh S, Geddes J, Swash M, Scaravilli F, Holton JL, Lashley T, Tomita T, Hashimoto T, Verkkoniemi A, Kalimo H, Somer M, Paetau A, Martin JJ, van Broeckhoven C, Golde T, Hardy J, Halktia M, Revesz T (2000) Variant Alzheimer's disease with spastic paraparesis and cotton wool plaques is caused by PS-1 mutations that lead to exceptionally high amyloid-beta concentrations. *Ann Neurol* **48**, 806-808.

[41] Martikainen P, Pikkarainen M, Pöntynen K, Hiltunen M, Lehtovirta M, Tuisku S, Soininen H, Alafauzoff I (2010) Brain pathology in three subjects from the same pedigree with presenilin-1 (PSEN1) P264L mutation. *Neuropathol Appl Neurobiol* **36**, 41-54.

[42] Takao M, Ghetti B, Hayakawa I, Ikeda E, Fukuuchi Y, Miravalle L, Piccardo P, Murrell JR, Glazier BS, Koto A (2002) A novel mutation (G217D) in the presenilin 1 gene (PSEN1) in a Japanese family: Presenile dementia and parkinsonism are associated with cotton wool plaques in the cortex and striatum. *Acta Neuropathol* **104**, 155-170.

[43] Verkkoniemi A, Somer M, Rinne JO, Myllykangas L, Crook R, Hardy J, Viitanen M, Kalimo H, Haltia M (2000) Variant Alzheimer's disease with spastic paraparesis: Clinical characterisation. *Neurology* **54**, 1103-1109.

[44] Wirths O, Weis J, Szczygielski J, Multhaup G, Bayer TA (2006) Axonopathy in an AβP/PS1 transgenic mouse model of Alzheimer's disease. *Acta Neuropathol* **111**, 312-319.